

# Phonon antibunching effect in coupled nonlinear micro/nanomechanical resonator at finite temperature

SHENGGUO GUAN<sup>1</sup>, WARWICK P. BOWEN<sup>2</sup>, CUNJIN LIU<sup>1</sup>, AND ZHENGLU DUAN<sup>1a</sup>

<sup>1</sup> College of Physics, Communication and Electrons, Jiangxi Normal University, Nanchang, 330022, China

<sup>2</sup> Center for Engineered Quantum Systems, School of Mathematics and Physics, The University of Queensland, St Lucia, Queensland 4072, Australia

PACS 81.07.0j – Nanoelectromechanical systems (NEMS)

PACS 42.50.Dv – Quantum state engineering and measurements

PACS 43.40.+s – Structural acoustics and vibration

**Abstract** –In this study, we investigate the phonon antibunching effect in a coupled nonlinear micro/nanoelectromechanical system (MEMS/NEMS) resonator at a finite temperature. In the weak driving limit, the optimal condition for phonon antibunching is given by solving the stationary Liouville-Von Neumann master equation. We show that at low temperature, the phonon antibunching effect occurs in the regime of weak nonlinearity and mechanical coupling, which is confirmed by analytical and numerical solutions. We also find that thermal noise can degrade or even destroy the antibunching effect for different mechanical coupling strengths. Furthermore, a transition from strong antibunching to bunching for phonon correlation has been observed in the temperature domain. Finally, we find that a suitably strong driving in the finite-temperature case would help to preserve an optimal phonon correlation against thermal noise.

**Introduction.** – Quantum state transfer and storage are crucial in quantum information processing. To date, the photon has been the information carrier most commonly used to transfer and store quantum information, and it has the advantage of high velocity, robustness to different environments, and good integrability. However, phonons, which are vibrational modes of mechanical resonators, can be maintained for a very long time before being eventually damped, and they have the ability to interact with a wide range of quantum systems, such as electric, magnetic, and optical systems. Therefore, phonons also have promising potential as quantum information carriers [1–3].

In quantum phononic networks, the nonclassical states of phonons or of a single phonon are important elements. Many methods to prepare nonclassical states of phonons or a single phonon have been proposed. For example, a single-phonon Fock state is prepared by two-phonon damping [4], a non-Gaussian state of a mechanical resonator is generated by performing measurements [5], and a single phonon is produced by the heralded measurement of the Stokes photon in cavity optomechanics [6, 7].

It is well known that a sufficiently high Kerr nonlinearity in an optical cavity will prevent further photons from entering once one photon is present, and this is called the photon blockade effect [8]. The transmitted light passing through the optical cavity then shows strong antibunching, which can be used to convert a coherent field into a train of single photons [9]. Similar to its optical counterpart, the phonon can also exhibit an antibunching effect in a strong nonlinear mechanical resonator [10–15]. However, the typical intrinsic nonlinearity of most micro/nanomechanical resonators is usually very weak [16–21]. Thus, we aim to determine whether strong phonon antibunching can be realized in a coupled micro/nanomechanical resonator system with weak intrinsic mechanical nonlinearity.

In fact, a similar problem of weak nonlinearity also exists in the optical case. To address this problem, Liew and Savona found that photons exhibit strong antibunching in a system consisting of two coupled optical cavities with weak optical nonlinearity, which is called the unconventional photon blockade (UPB). Ciuti *et al.* found that the underlying physics of UPB is that the excitation from the vacuum state to the two-photon state was suppressed by the destructive quantum interference between distinct

<sup>1a</sup> duanzhenglu@jxnu.edu.cn

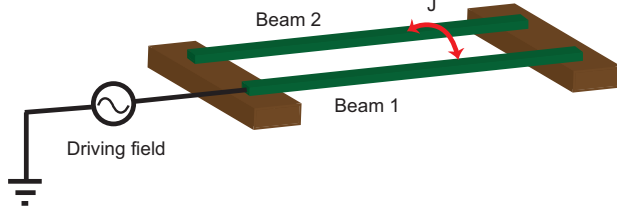


Fig. 1: (Color online) Schematic of the phonon blockade effect. A linear mechanical beam that is driven by an external force is linearly coupled to another nonlinear mechanical beam.

pathways with a small and finite nonlinearity in the auxiliary cavity [22–26].

Owing to the high resonant frequency of an optical cavity, the thermal photon number is negligible at room temperature. Therefore, the effect of thermal photons on the photon statistics and correlations is usually neglected safely. However, for mechanical resonators, the thermal phonon number is not negligible, and significantly influences the phonon blockade even at temperatures of the order of several milliKelvins [11, 12, 27]. Hence, an analytical study of phonon antibunching may help to give a deeper insight into the quantum correlation at finite temperature.

Motivated by these above-mentioned studies, we propose a scheme to realize a strong phonon antibunching effect by coupling a linear micro/nanoelectromechanical system (MEMS/NEMS) resonator to a weakly nonlinear MEMS/NEMS resonator. The optimal conditions required to observe strong phonon antibunching in this system are analytically found at finite temperature based on the stationary Liouville-Von Neumann master equation. In particular, we systematically study the effect of the thermal noise on the quantum statistic and correlation properties. We expect our system to be useful for generating a nonclassical phonon state at finite temperature.

**Model.** – As shown in Fig. 1, the system under consideration consists of two linearly coupled doubly clamped mechanical beams. One mechanical beam (referred to as resonator 1) is a linear resonator coherently driven by a force signal, and the other (referred to as resonator 2) contains a weak Duffing nonlinearity without driving. The mechanical nonlinearity can be intrinsic, such as geometric and material nonlinearity [16, 17], or it can be induced by coupling the mechanical oscillator to a low-dimensional auxiliary system, such as a plate capacitance [18], Cooper-pair boxes [28], polar molecules [29], and quantum dots [30]. As an example, the coupling between mechanical resonators could be achieved by applying a voltage between two electrodes patterned on the beams, which gives rise to a static intermodal coupling [31, 32], or by using a non-rigid anchor strain to mediate between the two beams [33]. As opposed to the latter case, dielectric intermode coupling can be tuned freely.

We assume that the resonator 1 is harmonically driven

by an external force with amplitude  $F$  and frequency  $\omega_d$ . The Hamiltonian for the described system is given by ( $\hbar = 1$ ):

$$H = \omega_1 \hat{b}_1^\dagger \hat{b}_1 + \omega_2 \hat{b}_2^\dagger \hat{b}_2 + J (\hat{b}_1^\dagger + \hat{b}_1) (\hat{b}_2 + \hat{b}_2^\dagger) + F (\hat{b}_1^\dagger e^{i\omega_d t} + \hat{b}_1 e^{-i\omega_d t}) + U (\hat{b}_2^\dagger + \hat{b}_2)^4, \quad (1)$$

where  $\hat{b}_j$  ( $\hat{b}_j^\dagger$ ) is the annihilation (creation) operator for the phonon mode of the  $j$ -th mechanical resonator with resonance frequency  $\omega_j$  and damp rate  $\gamma_j$  ( $j = 1, 2$ ).  $J$  is the coupling strength between two mechanical resonators, and  $U$  is the nonlinearity of the mechanical resonator 2. For simplicity without loss of physics, in the following, we assume that the mechanical resonators share the same frequency and decay rate, i.e.,  $\omega_1 = \omega_2 = \omega_0$  and  $\gamma_1 = \gamma_2 = \gamma$ . Further, we assume that the coupling strength  $J$  and the mechanical nonlinearity  $U$  are much smaller than the resonance frequency  $\omega_0$ . Under these assumptions, we can neglect the anti-rotating wave terms and rewrite the Hamiltonian as

$$H = \Delta \hat{b}_1^\dagger \hat{b}_1 + \Delta \hat{b}_2^\dagger \hat{b}_2 + J (\hat{b}_1^\dagger \hat{b}_2 + \hat{b}_2^\dagger \hat{b}_1) + F (\hat{b}_1^\dagger + \hat{b}_1) + U \hat{b}_2^{\dagger 2} \hat{b}_2^2, \quad (2)$$

where  $\Delta = \omega_0 - \omega_d$  is the detuning of the mechanical resonance frequency from the driving frequency. The Hamiltonian (2) describes a model of driven-dissipative coupled nonlinear mechanical resonators, which is mathematically similar to the optical counterpart in Ref. [26]. This Hamiltonian is the starting point of our calculation.

Unlike the situation of photon blockades, the environmental temperature usually has a significant influence on typical phonon statistics and correlation owing to the low energy of individual phonons. With the inclusion of the temperature factor, here, we use the Liouville-Von Neumann master equation for the density matrix

$$\begin{aligned} \frac{d\hat{\rho}}{dt} &= \hat{L}\hat{\rho} \\ &= -i[H, \hat{\rho}] + \sum_{n=1,2} \frac{\gamma}{2} \left[ (n_{th} + 1) D[\hat{b}_n] \hat{\rho} + n_{th} D[\hat{b}_n^\dagger] \hat{\rho} \right] \end{aligned} \quad (3)$$

with the Lindblad operator  $D[\hat{A}] \hat{\rho} = 2\hat{A}\hat{\rho}\hat{A}^\dagger - \hat{A}^\dagger\hat{A}\hat{\rho} - \hat{\rho}\hat{A}^\dagger\hat{A}$ . Here,  $n_{th} = (\exp(T_0/T) - 1)^{-1}$  is the average phonon number of the mechanical resonators at the temperature  $T$  (We assume that the temperatures of two nanomechanical beams are the same), and  $T_0 = \hbar\omega/K_B$  is the characteristic temperature of the system with the Boltzmann constant  $K_B$ . Here, we have neglected the pure dephasing of the resonators because the dephasing rates are usually much smaller than other decay rates [34].

In this case, the statistic properties of phonons for mechanical beam 1 are described by the equal-time second-order correlation function:

$$g^{(2)}(0) = \frac{\text{Tr}(\hat{b}_1^\dagger \hat{b}_1^\dagger \hat{b}_1 \hat{b}_1 \hat{\rho}_{ss})}{\left( \text{Tr}(\hat{b}_1^\dagger \hat{b}_1 \hat{\rho}_{ss}) \right)^2}, \quad (4)$$

where  $\hat{\rho}_{ss}$  is the steady-state density matrix by setting  $d\hat{\rho}/dt = 0$  in Eq. (3). In the calculation, we write  $\hat{\rho}$  as the density matrix  $\hat{\rho} = \sum_{m,n=0}^N \rho_{mn,m'n'} |mn\rangle \langle m'n'|$  on the basis of phonon number states  $|mn\rangle$ , where  $m$  denotes the phonon number in mechanical mode 1 and  $n$  denotes the phonon number in mechanical mode 2. To find the steady-state density matrix, we need to find the eigenmatrix  $\hat{\rho}_{ss}$  of superoperator  $\hat{L}$  when it has an eigenvalue of 0, i.e.,  $\hat{L}\hat{\rho} = \lambda\hat{\rho}$  ( $\lambda = 0$ ). Such an eigenvalue problem can be numerically solved using the method in Ref. [35]. In the numerical calculation, we set the phonon number  $n = 10, m = 10$ , which is sufficiently large to ensure the convergence of the results in this work.

### Results for Phonon Antibunching. –

*Zero temperature case.* Figure 2 shows the numerical result of the equal-time second-order correlation function as a function of the nonlinearity  $U$  and mechanical coupling  $J$  at zero temperature. We observe that the phonon antibunching effect occurs in the parameter regime where the product  $JU$  is relatively small. Importantly, as opposed to the conventional phonon blockade effect, in this coupled-mechanical oscillator system, phonons exhibit antibunching even when the nonlinearity is negligible ( $U \ll \gamma$ ), although this is at the cost of a large  $J$ . In addition, in the regime of large  $U$  and  $J$ ,  $g^{(2)}(0)$  becomes extremely large, which means that phonons are superbunched.

To find the optimal condition for phonon antibunching, we analytically solve the steady-state master equation for the density matrix. Under the weak driving condition  $F \ll \gamma$ , the average mechanical excitations would be much lower than 1, and the Hilbert space of the total system can be truncated to  $m + n = 2$ . In this case, we denote  $|0, 0\rangle \rightarrow |1\rangle$ ,  $|0, 1\rangle \rightarrow |2\rangle$ ,  $|0, 2\rangle \rightarrow |3\rangle$ ,  $|1, 0\rangle \rightarrow |4\rangle$ ,  $|1, 1\rangle \rightarrow |5\rangle$ , and  $|2, 0\rangle \rightarrow |6\rangle$ . Hence, the density matrix operator  $\hat{\rho}$  can be written as  $\hat{\rho} = \sum_{m,n=1}^6 \rho_{mn} |m\rangle \langle n|$ . In addition, weak mechanical excitations would result in  $\rho_{00} \simeq 1 \gg \rho_{01}, \rho_{10} \gg \rho_{02}, \rho_{20}, \rho_{11}$ . Then, the equal-time second-order correlation function can be approximately expressed as:

$$g^{(2)}(0) \simeq \frac{2\rho_{66}}{\rho_{44}^2}. \quad (5)$$

Obviously, if  $\rho_{66} = 0$ , then  $g^{(2)}(0) = 0$ , which implies a low probability of having two phonons in the first mechanical mode. After performing tedious calculations using the perturbation theory, we obtained the expression for the matrix element  $\rho_{66}$  in the zero-temperature case ( $n_{th} = 0$ )

$$\rho_{66} = \frac{F^4 \left| U \left( J^2 + 2\tilde{\Delta}^2 \right) + 2\tilde{\Delta}^3 \right|^2}{2J^8 \left| U + 2\tilde{\Delta} \right|^2}. \quad (6)$$

where  $\tilde{\Delta} = \Delta - i\gamma/2$ . In the calculation, we further assume a large mechanical coupling  $J$ ; otherwise, the expression

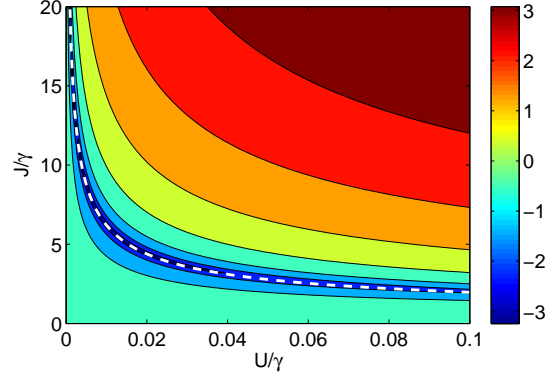


Fig. 2: (Color online) Equal-time second-order correlation function  $\log_{10}(g^{(2)}(0))$  as a function of the mechanical coupling  $J$  and the nonlinear coefficient  $U$  at zero temperature. The white dashed curve is calculated from the analytical optimal conditions Eqs. (7) and (8). The parameters are:  $\gamma = 1$ ,  $\Delta = 0.29\gamma$ , and  $F = 0.001\gamma$ .

for matrix elements would be more complicated. Then, we can find the following condition for perfect antibunching

$$2UJ^2 + 4(\Delta + U)\Delta^2 - (3\Delta + U)\gamma^2 = 0 \quad (7)$$

$$8U\Delta + 12\Delta^2 - \gamma^2 = 0 \quad (8)$$

which is mathematically the same as the results in the photon blockade case [26]. We plot the optimal condition in Fig. 2 (white dashed curve), which is in good agreement with the numerical result.

In the situation where the mechanical coupling  $J$  is much greater than the mechanical damping  $\gamma$ , the optimal parameters required to achieve  $\rho_{66} = 0$  can be approximated as

$$\Delta_{optimal} \simeq \frac{\gamma}{2\sqrt{3}} \quad (9)$$

$$U_{optimal} \simeq \frac{2\gamma^3}{3\sqrt{3}J^2} \quad (10)$$

Obviously, in this case, the nonlinearity that is required to observe an optimal blockade can be made extremely small ( $U_{optimal}/\gamma = 2\gamma^2/(3\sqrt{3}J^2) \ll 1$ ), contrary to the condition of conventional phonon blockade ( $U/\gamma \gg 1$ ).

We then study the phonon number probability distribution  $P_m = \sum_{n=0}^{\infty} \rho_{mn,mn}$  of mechanical mode 1 when the phonon blockade occurs. For comparison, we also show the probability distribution of a coherent state with the same mean phonon number  $|\alpha|^2 = \sum_{m=0}^{\infty} P(m)$ , which obeys the Poisson distribution  $P(n) = |\alpha|^{2n} e^{-|\alpha|^2}/n!$ . As shown in Fig. 3, the largest probability is occupied by the vacuum state. The one-phonon state is the next most probable. The two-phonon state is significantly less probable than the single-phonon state. Compared to the coherent state (the same mean phonon number with the blockade case), the probability for the two-phonon state is small, which indicates that the state of mechanical mode

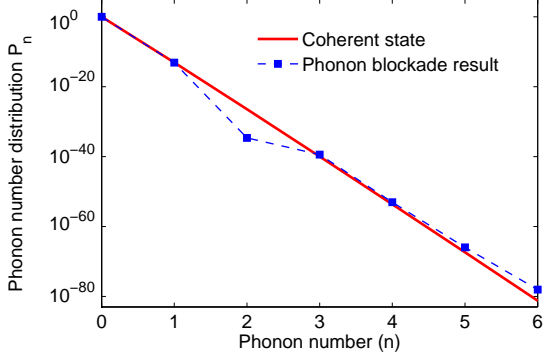


Fig. 3: (Color online) Population distribution of number state of phonon mode 1. The other parameters are:  $\gamma = 1$ ,  $U = 0.00387\gamma$ ,  $J = 10\gamma$ ,  $\Delta = 0.2874\gamma$ , and  $F = 0.00005\gamma$ .

1 has a nonclassical distribution. Recently, similar results have also been observed in optical counterparts [22].

*Finite temperature case.* In the previous subsection, we studied the phonon blockade effect without including the effect of environmental temperature. However, cooling a mechanical resonator down to zero temperature is not easy achieved experimentally. Therefore, it is important to study the phonon blockade at finite temperature. First, in Fig. 4, we numerically plot  $g^{(2)}(0)$  as a function of  $J$  and  $U$  at  $T = 0.04T_0$ . It can be seen that the phonon antibunching effect still exists in the weak nonlinearity  $U$ , but small mechanical coupling  $J$  regime (enclosed by the white solid line in Fig. 4). It is also observed that there is strong phonon antibunching in a specific regime, which is similar to that in the zero-temperature case. However, in the regime of weak nonlinearity  $U$  and large  $J$ ,  $g^{(2)}(0)$  is greater than 1, which is contrary to the zero-temperature case (see Fig. 2). This behavior indicates that thermal noise destroys the phonon antibunching effect in the regime of weak nonlinearity  $U$  and large  $J$ .

To study the effect of the environmental temperature on the phonon blockade, we present the analytical expressions of the density matrix elements  $\rho_{66}$  and  $\rho_{44}$  in the strong coupling regime (Using the same procedure as in the zero-temperature case):

$$\rho_{44} = \frac{F^2 |\tilde{\Delta}|^2}{|J^2 - \tilde{\Delta}^2|^2} + n_{th} \quad (11)$$

$$\rho_{66} = \frac{F^4 |U(J^2 + 2\tilde{\Delta}^2) + 2\tilde{\Delta}^3|^2}{2J^8 |U + 2\tilde{\Delta}|^2} + \frac{2F^2 |\tilde{\Delta}|^2}{J^4} n_{th} + (\frac{3}{4}n_{th}^2)$$

From Eqs. (11-12), both  $\rho_{44}$  and  $\rho_{66}$  contain two parts: one part determined by the temperature or the thermal phonon number, and the other part from the system itself (quantum interference). These two parts incoherently contribute to the phonon correlation. From Eq. (12), it

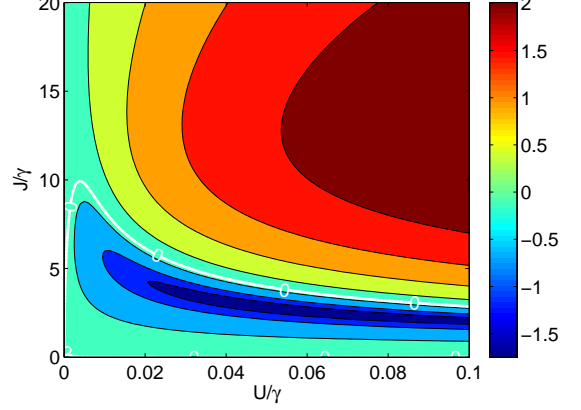


Fig. 4: (Color online) Equal-time second-order correlation function  $\log_{10}(g^{(2)}(0))$  as a function of mechanical coupling  $J$  and nonlinearity  $U$  at temperature  $T = 0.04T_0$ . The solid white line indicates the contour line with  $g^{(2)}(0) = 1$ . The other parameters are:  $\gamma = 1$ ,  $\Delta = 0.29\gamma$  and  $F = 0.001\gamma$ .

can be noted that  $\rho_{66} > 0$ , which implies that the perfect antibunching condition no longer exists at finite temperature. However, from Eq. (12) we can see that for a fixed temperature  $T$ , when the first term vanishes, the equal-time second-order correlation will take the minimal value. Therefore, the optimal condition for the strong phonon antibunching at finite temperature is the same as that at zero temperature. When the environmental temperature is small, the region for  $0 < g^{(2)}(0) < 1$  still exists because the quantum interference partially contributing to phonon correlation leads to an imperfect antibunching effect. When the mechanical coupling  $J$  is small, the contribution from quantum interference is enhanced, leading to a stronger phonon antibunching, and vice versa. These conclusions are well confirmed by the numerical results in Fig. 4.

Figure 5 shows  $g^{(2)}(0)$  as a function of the environmental temperature. Based on different behaviors of the second-order correlation function, the whole regime can be divided into three parts by two boundary temperatures  $0.028T_0$  and  $0.046T_0$ . In the first region (region I),  $g^{(2)}(0)$  is a constant and is much smaller than 1, which means that the phononic mode has a strong antibunching effect. Therefore, we called it the quantum regime. Interestingly, the quantum correlation is hardly affected by the thermal noise in the quantum regime, which is very helpful to experimentally observe the strong phonon antibunching at low finite temperature. In the second region (region II),  $g^{(2)}(0)$  experiences a sharp increase from  $3 \times 10^{-6}$  to 2 with increasing temperature. Obviously, in this regime, the quantum correlation of the phononic mode undergoes a transition from strong antibunching to bunching. We call it the crossover regime. In the third region (region III),  $g^{(2)}(0)$  approaches another constant 2, which means that the phononic mode has the statistic property of a thermal field. This regime is called the thermal regime.

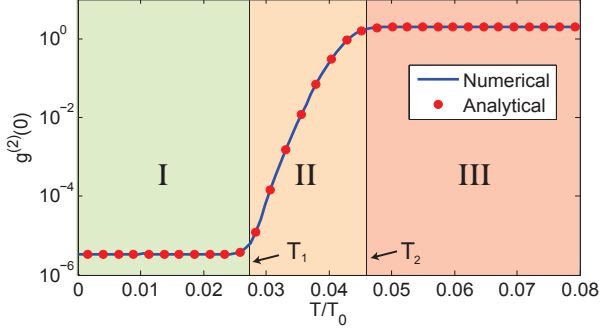


Fig. 5: (Color online) Equal-time second-order correlation function  $g^{(2)}(0)$  as a function of environmental temperature  $T$ . I, II, and III represent the quantum regime, crossover regime, and thermal regime, respectively. The numerical result is obtained based on the steady-state master equation (3), and the analytical result is calculated based on Eqs. (5, 11, 12). The parameters that are used in this figure are:  $\gamma = 1$ ,  $U = 0.00096\gamma$ ,  $J = 20\gamma$ ,  $\Delta = 0.2885\gamma$ , and  $F = 0.01\gamma$ .

These phenomena described in last paragraph can be explained from Eq. (5) and (12) as follows. In the quantum regime, the first term is much larger than other terms in Eq. (12), i.e., quantum interference dominates, and therefore,  $g^2(0)$  mainly shows the pure quantum correlation. In the thermal regime, the third term is much larger than other terms in Eq. (12), i.e., pure thermal noise dominates, which results in  $g^{(2)}(0) \approx 2$ . In the crossover regime, the gradually enhanced thermal noise gradually suppresses and eventually destroys the quantum correlation; hence,  $g^2(0)$  monotonously increases from an almost vanishing value to 2. Two critical temperatures can be determined as follows: when the first term is equal to the second term and much greater than the third term in Eq. (12), the corresponding temperature is the first boundary value. Then, we find  $T_1 = T_0 / \ln \left( 1 + 4J^4 |U\tilde{\Delta} + 2\tilde{\Delta}^2|^2 / F^2 |U(J^2 + 2\tilde{\Delta}^2) + 2\tilde{\Delta}^3|^2 \right)$ ; when the third term is equal to the second term and much greater than the first term in Eq. (12), we find another boundary temperature  $T_2 = T_0 / \ln \left( 1 + J^4 / 2 |F\tilde{\Delta}|^2 \right)$ .

We also studied the second-order correlation function versus the time delay  $g^{(2)}(\tau)$  at three different environment temperatures, as shown in Fig. 6. Owing to the probability oscillation between the phonon state  $|0, 1\rangle$  and  $|1, 0\rangle$ , the second-order correlation functions oscillate with period  $2\pi/J$ . In the zero-temperature case (Fig. 6(a)), the value of  $g^{(2)}(0)$  becomes negligible. For  $T = 0.043T_0$  (Fig. 6(b)), the amplitude of the oscillation of  $g^{(2)}(\tau)$  decreases; meanwhile, the value of  $g^{(2)}(0)$  increases to unitary. When the temperature is further increased to  $T = 0.1T_0$  (Fig. 6(c)), the value of  $g^{(2)}(0)$  is  $\simeq 2$ , indicating that the phonon field in the mechanical resonator 1 is a thermal field. Again, the time evolution of the second-order correlation function shows that a large thermal noise

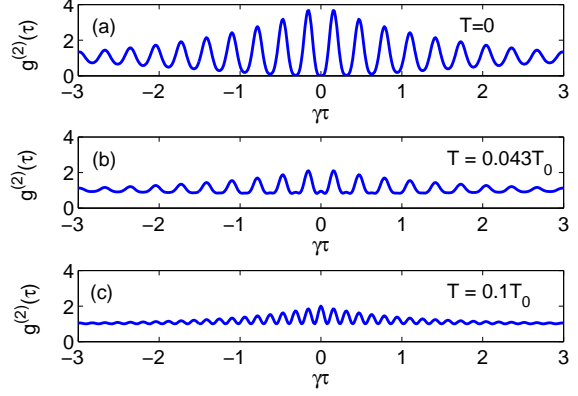


Fig. 6: (Color online) (a-c) Second-order correlation function  $g^{(2)}(\tau)$  is plotted as a function of time delay  $\tau$  at different temperatures. The parameters used in this figure are:  $\gamma = 1$ ,  $U = 0.00096\gamma$ ,  $J = 20\gamma$ ,  $\Delta = 0.288\gamma$ , and  $F = 0.01\gamma$ .

will suppress and even destroy the phonon antibunching. From Fig. 6, one can see that strong phonon antibunching is demonstrated in a range about  $\pi/J$  around the zero-delay, which gives a limited requirement for the temporal resolution of a detector.

We then investigate the influence of the driving force on the phonon statistics. In Fig. 7, we plot  $g^{(2)}(0)$  of the phononic mode in mechanical resonator 1 as a function of the driving force at zero and finite temperatures. First, we focus on the zero-temperature case. From Eqs. (5), (11), and (12) we can obtain the equal-time second-order correlation function at zero temperature:

$$g^{(2)}(0) = \left| \frac{\left( U \left( J^2 + 2\tilde{\Delta}^2 \right) + 2\tilde{\Delta}^3 \right) \left| J^2 - \tilde{\Delta}^2 \right|^2}{\left( U + 2\tilde{\Delta} \right) \left| \tilde{\Delta} \right|^2 J^4} \right|^2. \quad (13)$$

It should be noted that in the weak driving regime,  $g^{(2)}(0)$  is independent of  $F$ , and is consistent with the numerical result shown in Fig. 7. However, the analytical result clearly deviates from the numerical result in the strong driving regime. It is shown that the analytical result is valid only in the weak driving regime. The reason is that a strong driving enhances the population in the high phonon number states, and therefore decreases the antibunching effect.

Next, we discuss the influence of the driving amplitude  $F$  on  $g^{(2)}(0)$  in the finite-temperature case. As opposed to the zero-temperature case, it can be seen that all second-order correlation curves at finite temperature first decrease and then increase as the driving force is enhanced. Indeed, a similar phonon correlation behavior was numerically observed without physical interpretation in Ref. [13]. In the weak driving limit, the analytical model well reproduces the numerical calculation. However, because the analytical model is based on the assumption that the total

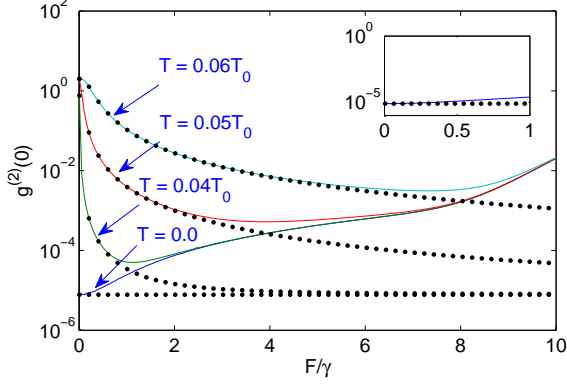


Fig. 7: (Color online) Equal-time second-order correlation function  $g^{(2)}(0)$  versus the driving strength  $F$  at different temperatures. The dotted line represents analytical results, and the solid line represents the numerical results. The inset is the zero-temperature case. The other parameters are:  $\gamma = 1$ ,  $U = 0.00096\gamma$ ,  $J = 20\gamma$ ,  $\Delta = 0.288\gamma$ .

phonon number is small ( $m + n = 2$ ), it fails to reproduce the increasing  $g^{(2)}(0)$  at higher driving. These observations can be understood from Eqs. (5), (11), and (12). When  $F$  is very small, the thermal noise term dominates the matrix elements  $\rho_{44}$  and  $\rho_{66}$ , and hence, the phonon state is approximately a thermal state ( $g^{(2)}(0) \approx 2$ ). With the increase in driving strength, the contributions from the quantum-interference terms in Eqs. (11) and (12) become important, leading to a decrease in  $g^{(2)}(0)$ . When the driving is sufficiently strong, the three and higher phonon states in resonator 1 are populated with increased probability owing to the strong coupling between resonator 1 and resonator 2. Hence, the second-order correlation function will increase again, resulting in a degradation of phonon antibunching. From the above discussions, it is clear that a very weak force is required to achieve a stronger antibunching effect for the zero-temperature case, while a suitably strong driving strength is helpful to preserve the stronger phonon antibunching effect when thermal noise exists.

Now, we discuss the experimental feasibility to observe the phonon blockade effect in the presence of unavoidable thermal noise. We assume that the two resonators in our model are silicon-based MEMS/NEMS resonators, which are doubly clamped rectangular cross-section beams with width  $d = 5$  nm and length  $L = 100$  nm. According to Ref. [17, 32], we find that the fundamental frequency is  $\omega_0/2\pi = d/L^2\sqrt{E/\rho} = 4.3$  GHz and the nonlinear strength  $U = \hbar(1.6\rho d^4L)^{-1} = 430$  Hz. The decay rate of the resonator is dependent on many factors, such as the geometrical configuration, anchor loss, environmental pressure and temperature, input-output loss, and thermoelastic damping. With a suitable design and fabrication, the total decay can be controlled. For simplicity, we take a typical value of  $\gamma = 10$  MHz, which corresponds to a quality factor  $Q \sim 4300$ . If we assume the coupling

between two mechanical resonators comes from an electrostatic force, the coupling strength  $J$  can be freely adjusted by changing the externally applied voltage. With these feasible parameters, we can then estimate the characteristic temperature  $T_0 = \hbar\omega_0/K_B \sim 196$  mK. According to the previous discussion, for an environmental temperature below 5.3 mK, the phonon blockade is almost unaffected by the thermal noise. Such a temperature is attainable using current laboratory technology. To measure the time-delayed second-order correlation function  $g^{(2)}(\tau)$ , we can adapt the same method as in Ref. [36]. In this reference [36], the phonon correlation can be transferred to the photon correlation, which can be measured by a typical photonic Hanbury Brown and Twiss (HBT) set-up. Here, we take coupling strength  $J = 20\gamma \sim 200$  MHz, corresponding to a window width of phonon antibunching  $\pi/J \sim 10$  ns. Apparently, this time scale is much greater than a typical temporal resolution of the detector (usually  $< 100$  ps) [37].

**Conclusion.** – We studied the phonon antibunching effect in a coupled mechanical resonator system with weak mechanical nonlinearity both at zero and finite temperatures. In the weak driving limit, analytical results were derived for the phonon antibunching in the strong coupling regime, and the temperature effect on the phonon blockade was investigated based on the stationary master equation. The results show that there exists a perfect phonon antibunching when the system parameters take the optimal conditional value at zero temperature. When thermal noise exists, the perfect antibunching condition is destroyed, leading to a suppressed phonon antibunching effect in the regime of small mechanical coupling, or leading to a destroyed phonon antibunching in the regime of large mechanical coupling. Furthermore, we find that the thermal noise has a different effect on the phonon correlation in the quantum regime, crossover regime, and thermal regime. Temperature variations have a negligible influence on the quantum correlation of the phonon mode when the environmental temperature is present in the quantum regime. Finally, the effect of the driving force on the phonon blockade is also discussed. It is found that a suitably strong driving, rather than a very weak driving, would help to preserve an optimal phonon antibunching effect at finite temperature.

\*\*\*

This work is supported by the National Natural Science Foundation of China under Grants No. 11364021 and No. 11664014, Natural Science Foundation of Jiangxi Province under Grant 20161BAB201023. W.P. Bowen acknowledges support from the Australian Research Council through grants CE110001013 and FT140100650.

## REFERENCES

- [1] S.J. HABRAKEN, K. STANNIGEL, M.D. LUKIN, P. ZOLLER, and P. RABL, *New J. Phys.*, **14** (115004) 2012.
- [2] M.V. GUSTAFSSON, T. AREF, A.F. KOCKUM, M.K. EKSTROM, G. JOHANSSON, AND P. DELSING, *Science*, **346** (207) 2014.
- [3] S. RIPS AND M.J. HARTMANN, *Phys. Rev. Lett.*, **110** (120503) 2013.
- [4] K. BORKJE, *Phys. Rev. A*, **90** (023806) 2014.
- [5] M.R. VANNER, I. PIKOVSKI, G.D. COLE, M.S. KIM, C. BRUKNER, K. HAMMERER, G.J. MILBURN, AND M. ASPELMEYER, *Proc. Natl. Acad. Sci. U.S.A.*, **108** (16182) 2011.
- [6] R. RIEDINGER, S. HONG, R.A. NORTE, J.A. SLATER, J.Y. SHANG, A.G. KRAUSE, V. ANANT, M. ASPELMEYER, AND S. GROBLACHER, *Nature*, **530** (313) 2016.
- [7] C. GALLAND, N. SANGOUARD, N. PIRO, N. GISIN, AND T.J. KIPPENBERG, *Phys. Rev. Lett.*, **112** (143602) 2014.
- [8] A. IMAMOGLU, H. SCHMIDT, G. WOODS, AND M. DEUTSCH, *Phys. Rev. Lett.*, **79** (1467) 1997.
- [9] I. CARUSOTTO AND C. CIUTI, *Rev. Mod. Phys.*, **85** (299) 2013.
- [10] N. DIDIER, S. PUGNETTI, Y.M. BLANTER, AND R. FAZIO, *Phys. Rev. B*, **84** (054503) 2011.
- [11] Y.X. LIU, A. MIRANOWICZ, Y.B. GAO, J. BAJER, C.P. SUN, AND F. NORI, *Phys. Rev. A*, **82** (032101) 2010.
- [12] A. MIRANOWICZ, J. BAJER, N. LAMBERT, Y.X. LIU, AND F. NORI, *Phys. Rev. A*, **93** (013808) 2016.
- [13] X.W. XU, A.X. CHEN, AND Y.X. LIU, *Phys. Rev. A*, **94** (063853) 2016.
- [14] H. SEOK AND E.M. WRIGHT, *Phys. Rev. A*, **95** (053844) 2017.
- [15] X. WANG, A. MIRANOWICZ, H.R. LI, AND F. NORI, *Phys. Rev. A*, **93** (063861) 2016.
- [16] G.W. DENG, D. ZHU, X.H. WANG, C.L. ZOU, J.T. WANG, H.O. LI, G. CAO, D. LIU, Y. LI, M. XIAO, G.C. GUO, K.L. JIANG, X.C. DAI, AND G.P. GUO, *Nano Lett.*, **16** (5456) 2016.
- [17] A.N. CLELAND, M.L. ROUKES, *J. Appl. Phys.*, **92** (2758) 2002
- [18] T. VEIJOLA AND T. MATTLA, *Int. J. RF Microwave Comput.-Aided Eng.*, **11** (310–321) 2001
- [19] V. PEANO AND M. THORWART, *New J. Phys.*, **8** (21) 2006.
- [20] E. BABOURINA-BROOKS, A. DOHERTY, AND G.J. MILBURN, *New J. Phys.*, **10** (105020) 2008.
- [21] I. KATZ, A. RETZKER, R. STRAUB, AND R. LIFSHITZ, *Phys. Rev. Lett.*, **99** (040404) 2007.
- [22] H. FLAYAC AND V. SAVONA, *Phys. Rev. A*, **96** (053810) 2017.
- [23] T.C.H. LIEW AND V. SAVONA, *Phys. Rev. Lett.*, **104** (183601) 2010.
- [24] X.W. XU AND Y.J. LI, *J. phys. B: At. Mol. Opt. Phys.*, **46** (035502) 2013.
- [25] D. GERACE AND V. SAVONA, *Phys. Rev. A*, **89** (031803(R)) 2014.
- [26] M. BAMBA, A. IMAMOGLU, I. CARUSOTTO, AND C. CIUTI, *Phys. Rev. A*, **83** (021802(R)) 2011.
- [27] P. KOMAR, S.D. BENNETT, K. STANNIGEL, S.J. M. HABRAKEN, P. RABL, P. ZOLLER, AND M.D. LUKIN, *Phys. Rev. A*, **87** (013839) 2013.
- [28] S. ETAKI, M. POOT, I. MAHBOOB, K. ONOMITSU, H. YAMAGUCHI, AND H.S. VAN DER ZANT, *Nat. Phys.*, **4** (785) 2008.
- [29] A. ANDRE, D. DEMILLE, J.M. DOYLE, M.D. LUKIN, S.E. MAXWELL, P. RABL, R.J. SCHOELKOPF, AND P. ZOLLER, *Nat. Phys.*, **2** (636) 2006.
- [30] K. SRINIVASAN AND O. PAINTER, *Nature (London)*, **450** (862) 2007.
- [31] T. FAUST, J. RIEGER, M.J. SEITNER, J.P. KOTTHAUS, AND E.M. WEIG, *Nat. Phys.*, **9** (485) 2013.
- [32] S. BARZANJEH AND D. VITALI, *Phys. Rev. A*, **93** (033846) 2016.
- [33] H. OKAMOTO, A. GOURGOUT, C.Y. CHANG, K. ONOMITSU, I. MAHBOOB, E.Y. CHANG, AND H. YAMAGUCHI, *Nat. Phys.*, **9** (480) 2013.
- [34] A.D. O'CONNELL, M. HOFHEINZ, M. ANSMANN, R.C. BIALCZAK, M. LENANDER, ERIK LUCERO, M. NEELEY, D. SANK, H. WANG, M. WEIDES, J. WENNER, J.M. MARTINIS, AND A. N. CLELAND, *Nature*, **464** (697) 2010.
- [35] V. SAVONA, arXiv: 1302.5937(2013).
- [36] S. HONG, R. RIEDINGER, I. MARINKOVIC, A. WALLUCKS, S.G. HOFER, R.A. NORTE, M. ASPELMEYER, AND S. GROBLACHER, *Science*, **358** (203) 2017.
- [37] X. DING, Y. HE, Z.C. DUAN, N. GREGERSEN, M.C. CHEN, S. UNSLEBER, S. MAIER, C. SCHNEIDER, M. KAMP, S. HOFLING, C.Y. LU, AND J.W. PAN, *Phys. Rev. Lett.*, **116** (020401) 2016.